**Astronomy & Astrophysics**

# Bright fibrils in Ca II K

A. Pietarila[1], J. Hirzberger[1], V. Zakharov[1], and S. K. Solanki[1,2]

[1] Max-Planck-Institut fur Sonnensystemforschung, 37191 Katlenburg-Lindau, Germany
 e-mail: pietarila@mps.mpg.de
[2] School of Space Research, Kyung Hee University, Yongin, Gyeonggi 446-701, Korea

**ABSTRACT**

*Context.* Except for the Ca II resonance lines, fibrils are ubiquitously present in most high-resolution observations of chromospheric lines.
*Aims.* We show that fibrils are also a prevailing feature in Ca II K, provided the spatial-resolution is sufficiently high.
*Methods.* We present high spatial resolution observations of an active region in the Ca II K line from the Swedish Solar Telescope. Through a comparison between photospheric intensity and magnetic field data, we study the connection between bright chromospheric fibrils and photospheric structures. Additionally, using Fourier analysis we study how the fibrils are linked to the observed dynamics.
*Results.* We find that very narrow, bright fibrils are a prevailing feature over large portions of the observed field. We also find a clear connection between the fibril footpoints and photospheric magnetic features. We show that the fibrils play two distinct roles in the observed dynamics: depending on their location they can act as a canopy suppressing oscillations or they can channel low-frequency oscillations into the chromosphere.
*Conclusions.* The Ca II K fibrils share many characteristics with fibrils observed in other chromospheric lines, but some features, such as the very small widths, are unique to these observations.

**Key words.** Sun: chromosphere – Sun: magnetic fields – Sun: oscillations

## 1. Introduction

The chromosphere is very inhomogeneous, both in space and time. When viewed in strong spectral lines, such as Hα, the presence of fibril-structures is evident everywhere. They are usually called spicules when located on the solar limb, mottles in the quiet Sun, and fibrils in active regions. Regardless of the name, these features are closely related to each other. Spicules carry a mass flux that is 100 times that of the solar wind into the lower corona (Withbroe 1983), making them an important factor in the mass balance of the solar atmosphere. The dynamic properties of many fibrils and spicules are consistent with the driver being photospheric oscillations that are leaking into the chromosphere along inclined magnetic field lines and forming shocks that in turn drive chromospheric jets (Hansteen et al. 2006). Hinode SOT observations have revealed a new subset of spicules which are even more dynamic, and for which a reconnection-related formation mechanism is a likely explanation (de Pontieu et al. 2007b). In addition, there are also heavily inclined, low-lying fibrils that are more static and do not show jet-like behavior (de Pontieu et al. 2007a). In all fibril types the observed structures (e.g., length) and dynamics (e.g., periodicity, lifetime) are clearly tied to the local magnetic field configuration.

Besides their ubiquitous presence in Hα, fibrils are seen in most chromospheric lines, e.g., Ca II 8542 Å (Vecchio et al. 2007; Cauzzi et al. 2008) and Ly-α 1216 Å (Patsourakos et al. 2007). However, prominent on-disk fibrils in the Ca II H and K lines are seldom observed. Bright and dark fibrils have been described by Zirin (1974) in narrowband (0.3 Å) Ca II K filtergrams of the quiet Sun and active regions (see also Marsh 1976), but more often observations of the Ca II K and H lines typically show long thin emission features, "straws" (Rutten 2007) only close

to the limb. On the disk observations usually show a structure of diffuse brightenings in magnetic regions and an even more complex pattern in quieter regions. In this paper we show that the fibril structures are ubiquitous in the Ca II K line as well, if observed at sufficiently high spatial resolution, and in a sufficiently narrow wavelength band to avoid contamination by photospheric radiation. The latter issue has been discussed in detail by Reardon et al. (2007).

The paper is organized as follows: in the next section the data and its reduction as well as analysis are discussed in some detail. Then the results, bright Ca II K fibril structures, widths and dynamics, are presented. The results are discussed and put into context with observations of other spectral lines in Sect. 4. Finally, Sect. 5 summarizes the main results.

## 2. Observations, data reduction and analysis

A region close to solar disk center (AR 10966, $\mu = 0.99$) was observed at the Swedish Solar Telescope (SST, Scharmer et al. 2003a) on Aug. 9, 2007 from 13:31 to 14:12 UT in periodically excellent seeing conditions. The observations were made using the adaptive optics (AO, Scharmer et al. 2003b) simultaneously with a 1.5 Å wide Ca II K (centered at line core) and 1 nm wide continuum interference filter (centered at 395.37 nm). The analyzed Ca II K and continuum image sequences are composed of 165 frames (10 ms exposure time) each with a cadence of 15 s. The SOUP tunable birefringent filter (Title & Rosenberg 1981) was used to record the full Stokes profile of the photospheric Fe I 6302 Å line at six wavelength positions (−250, −150, −75, 0, 75 and 150 mÅ from line core) with a cadence of 123 s for the full set of 4 polarization states and for the six

positions. The SOUP images were reconstructed using speckle reconstruction (e.g., Weigelt 1977; de Boer 1996). Multi-object multi-frame blind deconvolution (MOMFBD, van Noort et al. 2005) and speckle reconstruction were independently applied to the interference filter data to obtain images with very high spatial resolution. The Fried parameters and hence the applied speckle transfer functions were estimated in dependence of the distance of the individual subfields from the lock point of the AO (see Puschmann & Sailer 2006).

The two different image reconstruction methods yield very similar results for the continuum images, but there is a discrepancy between the two in the Ca II K images: the MOMFBD results in images in which sharp fibrils lie on a more uniform hazy component, whereas the speckle reconstructed images do not show this uniform feature. In the following, only properties found in images from both reconstruction methods are discussed. Furthermore, we focus exclusively on the bright fibril structures and do not address the dark structures in the present study.

The pixel size of the Ca II K and continuum data is 0.033 × 0.033 arcsec and for the SOUP data 0.065 × 0.065 arcsec. The field of view (FOV) is roughly 60 × 60 arcsec for both the Ca II K and continuum data. It is a few arcseconds smaller for the SOUP data. In the best frames the spatial resolution of the reconstructed Ca II K and continuum images is diffraction limited (the Rayleigh limit for Ca II K is 0.1 arcsec). The spatial resolution of the SOUP images is somewhat lower, approximately 0.2 arcsec.

For the SOUP data instrumental polarization effects of the laboratory setup were measured with dedicated calibration optics and the telescope polarization was determined using a model developed by Selbing (2005). The thus deduced demodulation matrices were applied to the SOUP data resulting in the full Stokes vectors at six spectral positions for each pixel of the FOV. The Stokes profiles were inverted assuming a one-component-plus-straylight Milne-Eddington atmosphere using the inversion code, HeLiX (Lagg et al. 2004). The magnetic component of the obtained atmosphere includes the magnetic field vector, $\boldsymbol{B} = (|\boldsymbol{B}|, \gamma, \chi)$, where $\gamma$ is the field inclination with respect to the line of sight and $\chi$ is the azimuth angle of the magnetic field, as well as the magnetic filling factor, $\alpha$, and the line-of-sight flow velocity, $v$. In the straylight component, having filling factor $(1 - \alpha)$, the magnetic field vector is assumed to be zero and all other parameters are coupled to the values of the magnetic component. This is a particularly simple way of accounting for the fact that only part of the rather small resolution element is filled with fields and we do not know the local atmospheric structure, except that it is unlikely to be well represented by the quiet Sun. From the inversion results we calculated maps of the Doppler velocity, $v$, and of the longitudinal magnetic flux density, $|\boldsymbol{B}| \cos \gamma \cdot \alpha$, which are the two most robust quantities.

The Ca II K filter contribution function in the quiet Sun (FALC model of Fontenla et al. 1993) shows that most of the signal is coming from the upper photosphere (Fig. 1). In fact, 90% of the emission in a FALC atmosphere is coming from below 550 km. The contribution functions in Fig. 1 were calculated using the nLTE radiative transfer code of H. Uitenbroek (Uitenbroek 1998, http://www.nso.edu/staff/uitenbr/rh.html). The code uses the Multi-level Accelerated Lambda Iteration (MALI) formalism of Rybicki & Hummer (1991, 1992) and takes into account effects of partial frequency redistribution for the Ca II K line. Since no transmission curve was available for the Ca II K filter, the contribution function was calculated for a 1.5 Å wide rectangular bandpass centered at the
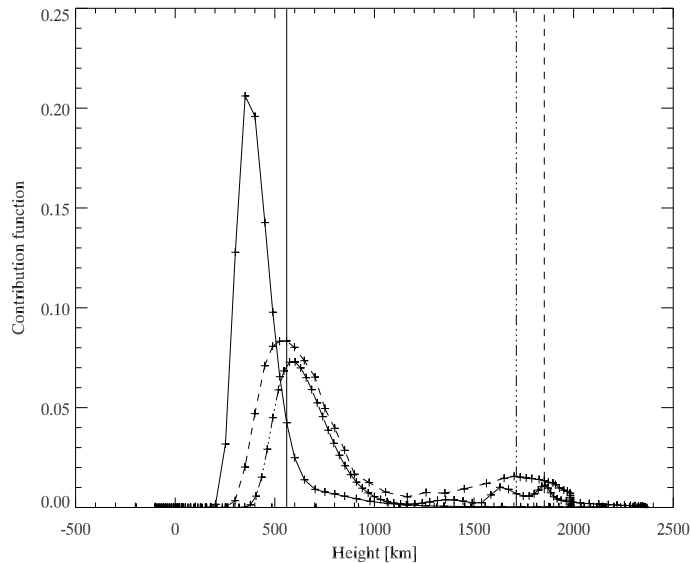


**Fig. 1.** Contribution functions for the Ca II K filter used in the observation for the FALC model (quiet Sun Fontenla et al. 1993, represented by the solid line), FALF model (network, Fontenla et al. 1993; in dashed line) and a Carlsson & Stein atmospheric model snapshot from a 1-dimensional radiative hydrodynamics simulation of a shock wave propagating through the formation region of the Ca II K line (Carlsson & Stein 1997; in dash-dotted line). The vertical dotted lines show the location from below which 90% of the contribution is coming. Units of the $y$-axis are arbitrary.

line core. The contribution function extends to the FALC chromosphere, but the chromospheric contribution is at best minor, especially at heights above 1000 km. In comparison, in regions such as the network and plage (described by FALF, i.e., model F of Fontenla et al. 1993) a much larger portion of the emission arises from the chromosphere, see dashed line in Fig. 1, which corresponds to the filter contribution function for the FALF model. Noticeable is the presence of a second peak in the middle to upper chromosphere. Also an upward propagating shock wave such as in the simulations of Carlsson & Stein (1997) produces a secondary chromospheric peak in the contribution function (dash-dotted line in Fig. 1). Consequently the data mainly sample the upper photosphere and temperature minimum region in quiet areas, but become sensitive to chromospheric features as soon as the temperature there is high, i.e., above photospheric magnetic features and above a hot canopy that may surround them. Note that Fig. 1 only gives a qualitative picture of the heights from which the emission in the Ca II K filter is coming, since none of the employed atmospheres can be deemed to be entirely realistic. The contribution functions presented here are comparable to the response functions presented by Carlsson et al. (2007) for the Hinode SOT Ca II H filter. That filter is somewhat wider than the filter used in this study and, consequently, the chromospheric contributions are slightly smaller.

To isolate the bright fibrils in the intensity images the following procedure was applied to 12 of the highest quality Ca II K images. First an intensity threshold was applied (5000–17 000 counts) and the resulting image was filtered with an unsharp mask (radius 5 pixels). Next a second threshold was applied (210–1990 counts) and the resulting image was converted from float to binary. The standard IDL procedure label_region was run on the binary image. The procedure labels each region (a non-zero valued pixel and all the adjacent neighboring non-zero
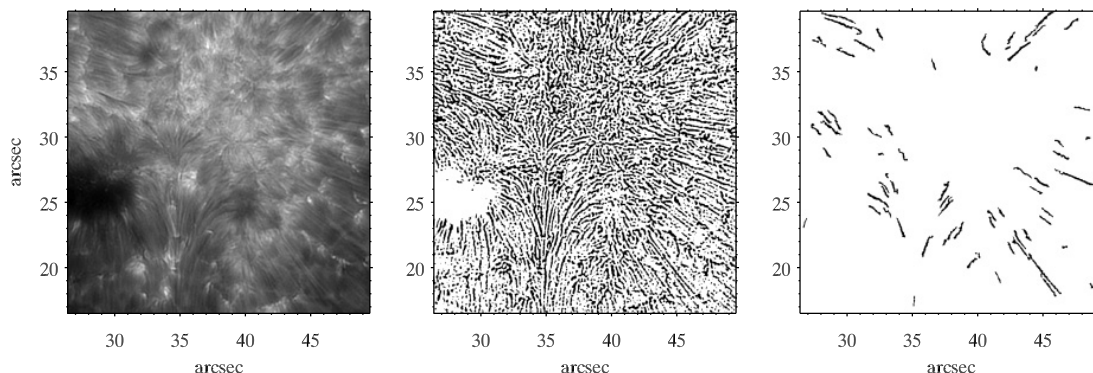
**Fig. 2.** Automatic detection of fibrils. See text for details. First image: original intensity image (linear color scale). Second: first binary image. Third: identified fibril segments.

pixels) in the image. Each of the labeled regions were studied individually and ones fulfilling certain criteria were kept. The criteria were: the region must consist of at least 60 pixels. The longest distance between two points must be at least 25 pixels. These two criteria are used to remove features that are too small in size. Additional criteria include the ratio of the circumference of the region to the longest distance between two points in the region must be less than 2.8. In addition, the edges of each region were identified and the slope between adjacent pixel pairs computed. Only regions, where the ratio of the mean of the absolute value of the slope and the standard deviation is larger than 0.9, are kept. These last criteria are employed to remove features that are not fairly straight and elongated, e.g., granule edges. The regions in the resulting binary image are again identified with the label_region procedure and regions with more than 55 pixels are identified as segments of fibrils. The method outlines the fibrils and enables computation of their widths. The masking and criteria were found through trial and error. In Fig. 2 are shown a portion of an original image, the first binary image, and the identified segments. The procedure creates only very few false identifications, but it misses many fibrils. Nonetheless, the 12 processed images resulted in nearly 6000 bright fibril segments and the properties of the segments are consistent in all the images. This confirms that the detection method is not sensitive to small changes in spatial resolution provided that the spatial resolution of the original images is sufficiently high.

A second way, entirely independent of the above described algorithm, to define fibril widths is to manually identify the edges of a fibril segment from the intensity images and calculate the width from that (shortest distance between the segment edges). This was done for four regions of a single snapshot, and served mainly to compare with and test the results obtained with the automated method. No measurements of full width at half maximum were made because the background intensity pattern also varies on very small scales and in many places the fibrils overlap each other.

To sketch out the large scale structure of the fibrils a Ca II K intensity image was divided into sections of $100 \times 100$ pixels ($3.3'' \times 3.3''$). Then each section was displayed and a dominant fibril direction was determined by eye. If no fibrils were present, no direction was determined. This was done for two intensity snapshots taken 36.5 min apart. The two images were chosen since they have the best spatial resolution and are located far away from each other in time.

To study the spatial properties of intensity oscillations standard Fourier techniques were used. We applied the Fourier transform on intensity fluctuations normalized to the temporal mean.

Without such a normalization the power maps would be dominated by intensity fluctuations of the highest intensity pixels. The resulting power spectra are divided into three frequency regions: 0.4–1.6 mHz, 2.4–4 mHz and 5.2–8 mHz. The first frequency region encompasses the long time evolution (>15 min), the second is dominated by the photospheric 5 min oscillations (normally filtered out by the acoustic cutoff frequency in the chromosphere), and the third one is (often considered mainly chromospheric) oscillations above the acoustic cutoff frequency. Because varying seeing conditions cause peaks in the power spectra it is not possible to compare the power in different frequency ranges. However, since the effect of the seeing is roughly the same for the continuum and Ca II K intensities in all the pixels, it is still possible to compare different spatial regions.

## 3. Descriptive results

### 3.1. Large scale pattern

The observed region is a decaying active region, AR 10966, located close to disk center. In continuum intensity the center of the FOV is dominated by a pore surrounded by plage (Fig. 3) where many of the intergranular lanes are filled with bright filigree. A second pore is located in the upper left corner of the FOV. The darker regions in the plage are micropores. Some isolated bright points are located in the quiet Sun at the lower and right edges of the FOV. The agreement between the photospheric intensity and the photospheric magnetic field obtained from a Milne-Eddington inversion (Fig. 4) is good: nearly all of the bright photospheric emission can be identified as regions with significant magnetic flux. Most of the FOV is unipolar though small patches of opposite polarity are present in the upper left corner in between the two pores and also below the central pore in the middle of the FOV. The pores are nearly isolated from the plage: they are surrounded by a layer of granulation with very little magnetic flux. Only the upper right corner of the central pore is directly connected to the plage. The granulation pattern is abnormal throughout most of the plage region, being composed of particularly small granules and intergranular lanes filled with filigree. Often, but not always, the red-shift relative to the rest of the FOV covers more of the surface in the abnormal granulation than in the more quiet regions (Fig. 5). In addition, the downflow lanes in the abnormal granulation appear more patchy, with strong downflows restricted to individual point-like features.

The pores and plage are clearly visible in Ca II K intensity (Fig. 6). The most distinct chromospheric feature is the bright fibrils originating from magnetic regions. The end points of the
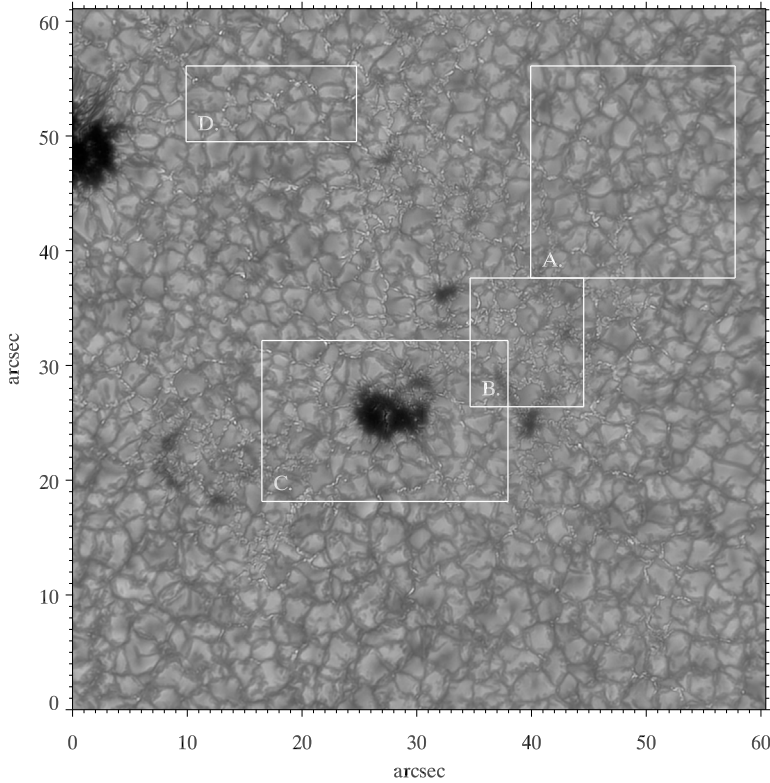
**Fig. 3.** Continuum intensity image obtained at 13:24:05–13:24:20 UT. The four boxes mark regions discussed later in the text. The color scale is linear.
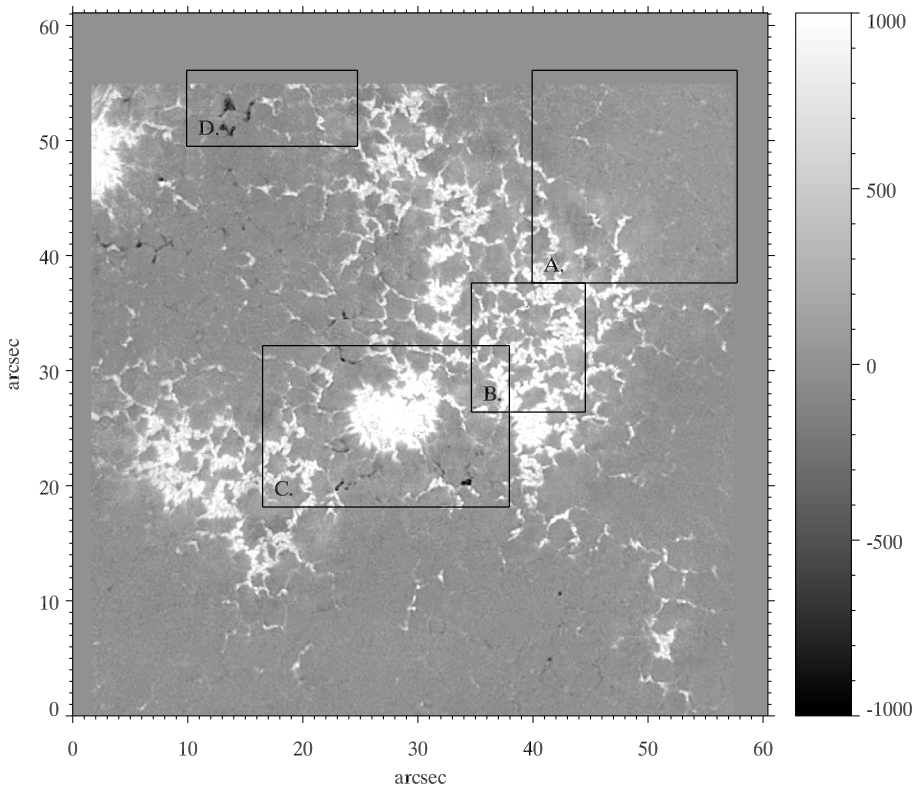


**Fig. 4.** As Fig. 3 but for the longitudinal magnetic flux (in G) in the photosphere. Note that this image, recorded at 13:25:12–13:27:19 UT, is not cotemporal with Fig. 3.

fibrils are cospatial with the photospheric bright points and magnetic concentrations. In the plage the stalky, short fibrils form a thick, carpet-like covering whereas at the plage edges the fibrils are longer, more organized and often nearly parallel to one another. The long fibrils extend over multiple granules and gradually fade out of view over the quiet Sun. The patch of network visible in the lower right corner of the FOV is also associated with fibrils which are much shorter than the fibrils originating from the plage edge. Outside the plage the dominant structure is reversed granulation (Cheung et al. 2007; Janssen & Cauzzi 2006).
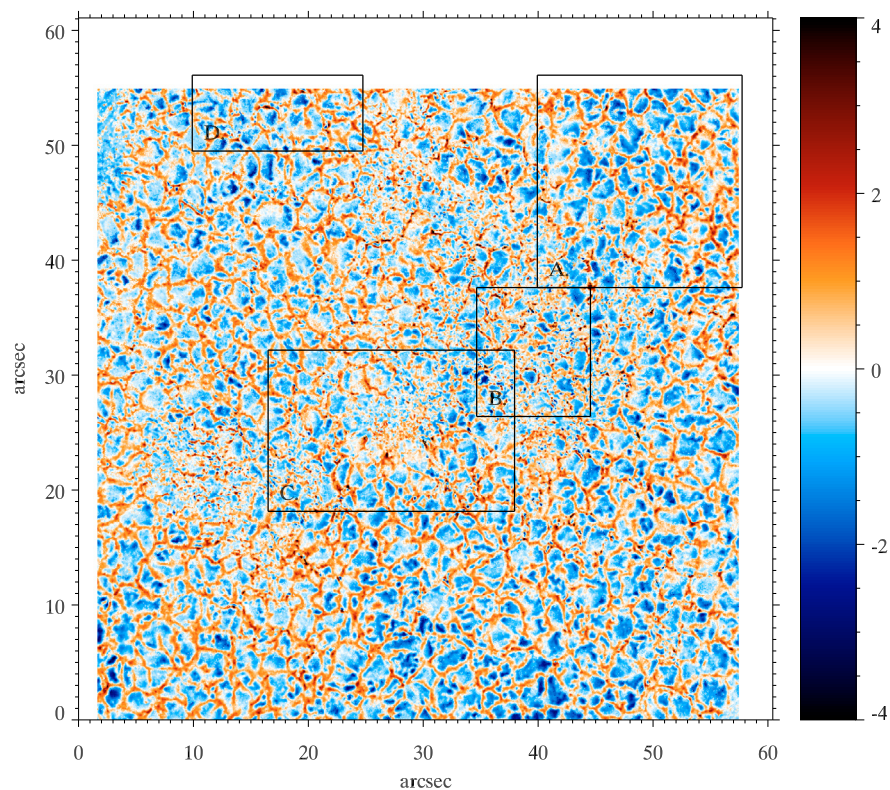
**Fig. 5.** As Fig. 3 but for the photospheric velocity (in km s$^{-1}$). Note that this image, recorded at 13:25:12–13:27:19 UT, is not cotemporal with Fig. 3.
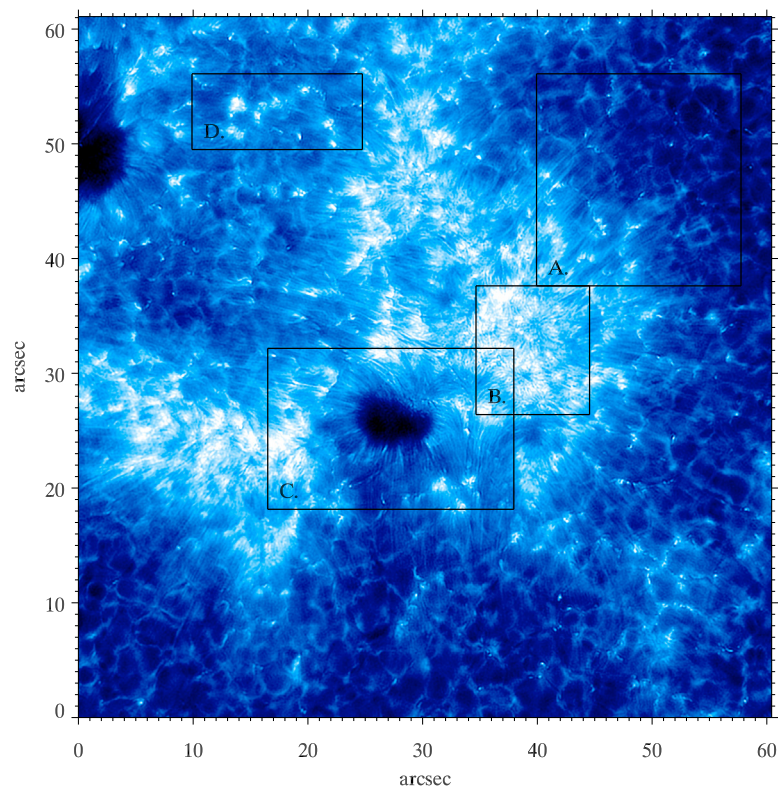


**Fig. 6.** As Fig. 3 but for Ca II K obtained at 13:24:05–13:24:20 UT. Color scale is linear.

The large-scale orientation pattern of the fibrils is shown in Fig. 7. The top most image is a binary image made by unsharp masking the Ca II K image with a 12-pixel wide filter and then thresholding it. The lower image shows the dominant fibril direction in each subregion, as discussed in the previous section. The fibrils extend (nearly radially) away from regions of strong magnetic field towards the quiet Sun. The center of the largest plage

(on upper right of the central pore) shows rosette-like structures with typical diameters of $\approx 10''$ (e.g., at $x = 42''$, $y = 30''$). The plage is more disorganized though even here most of the vectors are pointed towards quiet Sun. The fibrils do not display apparent large loop-like structures in this predominantly unipolar region observed at disk center. An exception is found in the upper left corner between the two pores where faint, small
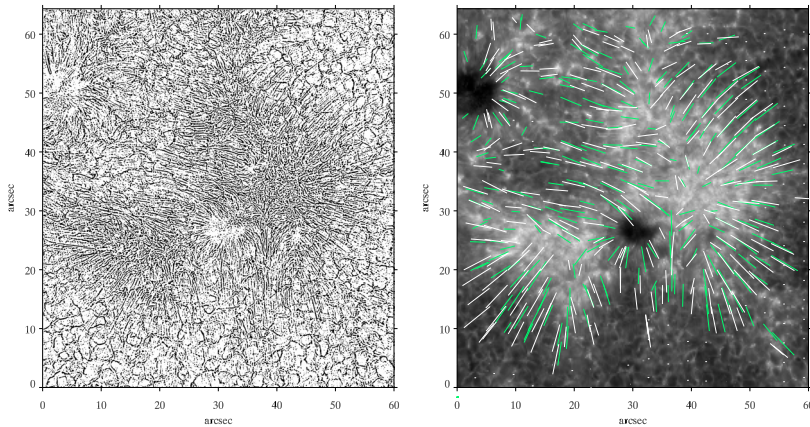
**Fig. 7.** *Left*: binary image of Ca II K. *Right*: Ca II K with over-plotted vectors showing prevalent direction of fibrils in the subregion. The green and white vectors are for images taken 36.5 min apart.
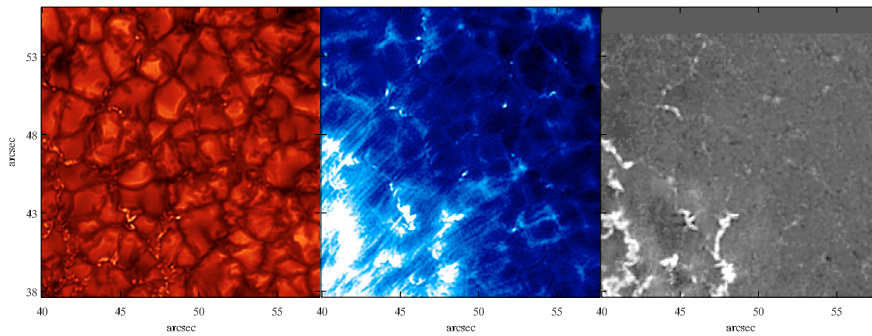


**Fig. 8.** Region A. *From left to right*: continuum intensity, Ca II K intensity, longitudinal magnetic flux. The magnetic flux color scale goes from –800 to 1000 G.

curved-structures are present. A granule surrounded by magnetic flux of the opposite polarity than most of the FOV is located here ($x = 13''$, $y = 52''$). Since the region is near disk center, curvature in the fibrils is more likely due to the non-potentiality of the magnetic field configuration than to the loops being inclined with respect to the line of sight. Since the central pore and the surrounding plage have the same polarity, no loops connecting the two are present. The region in between and below the plage and pore (located at $x = 34''$, $y = 24''$) has a very distinct cusp-like structure. There is a small patch of opposite polarity to the lower right of the pore which some of the cusp's fibrils connect to.

### 3.2. Fibril types

Four subregions (boxes in Figs. 3–6) sampling different environments were chosen for a more detailed study. Region A (plage edge and quiet Sun) has long fibrils extending over several granules. Region B is located in the middle of the plage. The cusp, i.e., fibrils originating from the pore and surrounding plage, is shown in region C. Small loop-structures connecting opposite magnetic polarities are present in region D.

#### 3.2.1. Region A: plage edge and quiet Sun

Region A (Fig. 8) is located at the edge of the plage. The lower left corner in the continuum image is covered with filigree and many fibrils originate from there. The denser the filigree, the more jumbled and packed together the fibrils are. The long fibrils originating from close to the plage edge are oriented towards the quiet Sun where no large concentrations of magnetic flux are present and reversed granulation is the dominant intensity pattern. The long fibrils are nearly parallel to one another. They can extend over several granules and also over filigree that is the foot point of additional fibrils. Fibrils do not originate from all the

bright points/filigree in the photosphere. In particular, the more isolated points in the quiet Sun are not associated with fibrils.

Closer inspection reveals that some of the apparent fibrils mirror the shape and location of photospheric filigree. Given the large contribution to the observed radiation from the photosphere (Sect. 2) these may actually be photospheric filigree shining through. Many, if not all, of the fibrils with kinks are such filigree. The transition from filigree to fibril is not an abrupt one: the photospheric filigree has the same shape in the continuum and Ca II K except that in Ca II K the filigree is often elongated/stretched towards the quiet Sun as it transitions into fibrils.

#### 3.2.2. Region B: strong plage

Region B (Fig. 9) is located in the strong plage. In the photosphere the intergranular lanes are filled with filigree and $\approx kG$-magnetic flux. The Ca II K image is covered by a carpet of short, stalky fibrils. The darker areas in the carpet, which correspond to the centers of the rosettes, can be identified as granule interiors. In the photospheric intensity and magnetic flux rosette-like structures are formed at the intersection of three or more granules whereas in the Ca II K rosette-like structures are formed in a granule that is surrounded at all sides by intergranular lanes filled with filigree. Overlapping structures complicate the identification of fibril endpoints, though the fibrils clearly originate from the magnetic flux-filled intergranular lanes. In places it appears as if the fibrils cross each other and are in lying several layers. An example is located in the lower left corner of Fig. 9 (at $\approx x = 36''$, $y = 28''$).

#### 3.2.3. Region C: pore and plage

There is no large difference between the sizes of the pore (darkening) in the continuum and Ca II K (compare the corresponding frames in Fig. 10). The small pore at the upper right of the large
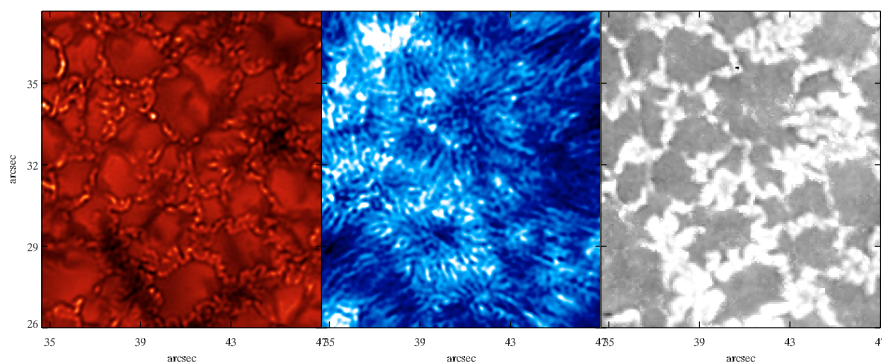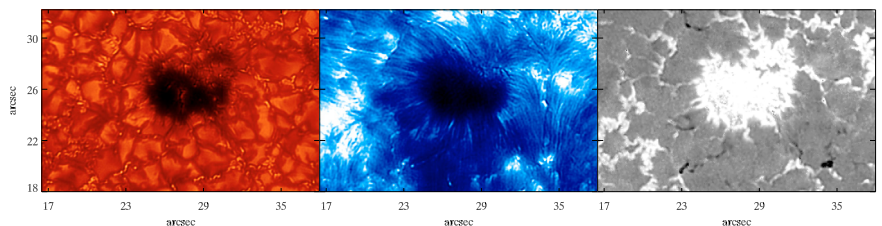
**Fig. 9.** Region B: as Fig. 8, but for region B.



**Fig. 10.** Region C. as Fig. 8, but for region C.
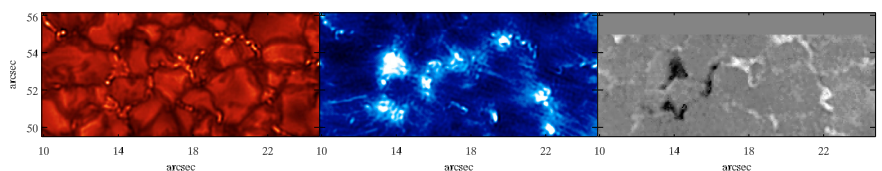


**Fig. 11.** Region D. as Fig. 8, but for region D.

pore is not well visible in Ca II K, although it is associated with a strong magnetic field (bottom panels in Fig. 10). Instead, in Ca II K the region is covered with short fibrils. Fibrils originating from the pore form a structure similar to a superpenumbra around the pore. The width of the superpenumbra is comparable to the radius of the pore, $\approx 3''$.

Fibrils in Region C (Fig. 10) are oriented away from the pore and plage. Since the two are of the same magnetic polarity, the fibrils form a cusp-like structure (at $[x = 34'', y = 22–26'']$), i.e., they are deflected from the nearly radial orientation to being mostly parallel to one another. A portion of the fibrils involved in forming the cusp connect to the small patch of opposite (negative) polarity below. The fibrils connecting to the opposite polarity have slightly different orientations and lengths. It appears as if the fibrils are not all in the same layer, but instead the fibrils connecting to the opposite polarity are lower in the atmosphere. There is another small negative polarity patch at $\approx [x = 34'', y = 30'']$ which appears to be an endpoint of some of the superpenumbral fibrils.

The large pore has a very clear superpenumbra in Ca II K emission except in the upper right corner where the pore is in direct contact with the plage. In the photosphere the granulation pattern in the corner is disrupted. The corner does not have a clear superpenumbra but instead it is more similar to the dense plage area than the rest of the pore, i.e., the Ca II K fibrils are more carpet-like. The magnetic flux in the plage is not much lower than in the pore. This may, however, be due to the high level of straylight which dominates in the umbra. The rest of the pore-superpenumbra boundary serves as the foot point to fibrils that are oriented nearly radially away from the pore. They can extend outside the superpenumbra indicating that some of the fibrils are located at a different height in the atmosphere than the bulk of the superpenumbra. Since the region is unipolar, the superpenumbra cannot connect back to the photosphere but instead must expand higher up and disappear from view. In contrast, some of the fibrils remain visible beyond the superpenumbra.

### 3.2.4. Region D: bipolar weak plage

Region D (Fig. 11) is located between the two pores. Some of the intergranular lanes are filled with filigree that have the same shape in the continuum and Ca II K images. The intergranular lanes surrounding one of the central granules are filled with filigree which coincides with magnetic flux of the opposite polarity than most of the FOV. The opposite polarity field is the foot point of fibrils that extend toward the directions of both pores and form small loop-structures which are best seen in unsharp masked images. The large scale structure of the fibrils is more disorganized than in other regions with a moderate (though still less than in the plage) amount of magnetic flux. Most of the surface in region D is covered by fibrils. This is best seen in Fig. 6. In regions with no filigree the fibrils are parallel to one another whereas in the filigree-filled regions they form rosettes similar (though not as dense) to the plage (region B).

It should be noted that in the current dataset fibrils cannot be used as a reliable means of determining the magnetic connectivity of the photosphere. For example, in the right side of regions D some of the long, clear fibrils appear as if they are connecting two features. However, inspection of the magnetic field reveals that these two features are of the same polarity and thus cannot be connected magnetically.

## 4. Fibril dimensions

The histogram of automatically detected bright fibril segment widths (Fig. 12) peaks at 0.11–0.14 arcsec (i.e., only slightly above the diffraction limit, indicating that the actual widths may be below 0.1 arcsec). The distribution goes down to values below the diffraction limit and up to 0.2 arcsec. No correlation is found between the fibril intensity and width. The lengths of the segments are comparable to the length scale of the reversed granulation (which is the underlying intensity pattern): most of the segments are less than 1.5 arcsec long. The lower limit of
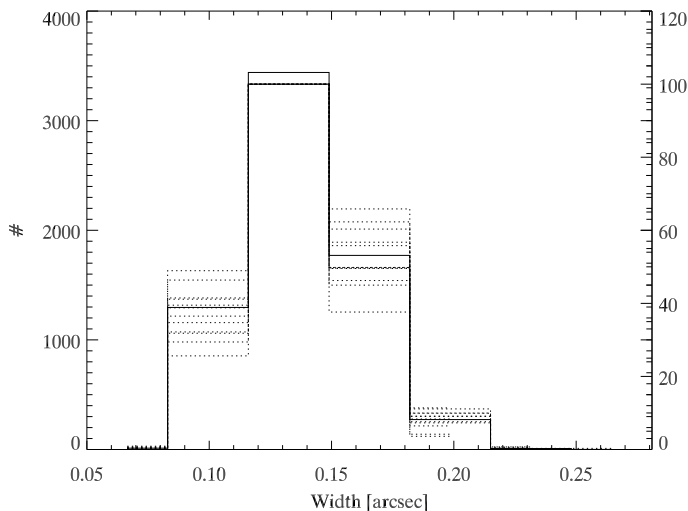
**Fig. 12.** Histogram of automatically detected fibril widths. The solid line is the average histogram for all 12 images, dotted lines for the individual images.

the lengths of the fibril segments is set by the criterion used in identification (0.825 arcsec).

The manually determined widths (Fig. 13) are very similar to the automatically detected widths: most fibrils are between 0.11 and 0.14 arcsec wide. There is a pattern in the spatial distribution of the widths: a larger portion of fibrils with widths below 0.14 and fewer wide fibrils are found in region C (pore). Most of the fibrils in region A are between 0.11 and 0.18 arcsec wide. Region D (weak bipolar plage) resembles region A except for the larger portion of widths larger than 0.18 arcsec. Region B (strong plage) has a wide distribution and fibrils with widths up to and over 0.2 arcsec are more common than in the other regions. Again, no correlation is found between the widths and the fibril intensities. However, the mean value of the widths in a region increases with increasing mean intensity (which in turn is correlated with the magnetic flux) of the whole region (not mean intensity of the fibrils), i.e., the fibrils are on average thicker in the plage than in the quiet Sun. If this effect is related to the width of the spectral filter employed for the observations is unclear: in the quiet Sun chromospheric layers contribute little to the observed intensity, so that fewer fibrils are visible and only the brighter central spines of the fibrils are seen. In regions with more magnetic flux more chromospheric contribution is obtained and also fainter parts of the fibrils are seen making them appear broader.

Interference from the underlying reversed granulation and lack of well defined fibril ends make measuring lengths difficult, and only a rough measurement was done by hand. Fibrils extending over quiet Sun are longest (from 6 up-to 10 arcsec) and fibrils in regions with more magnetic flux and stronger unipolar crowding are significantly shorter (1–1.5 arcsec).

## 5. Temporal evolution

The main intensity variation in the Ca II K images is in the middle photosphere and is due to reversed granulation. Because of this it is difficult to distinguish changes in fibril intensity from changes in the background intensity. This in turn makes it difficult to follow individual fibrils from one frame to the next.

A variety of dynamic phenomena such as splitting, merging, fading, brightening and elongation are seen in the fibrils.

The large scale structure is very stable throughout the observing sequence and does not change significantly over 36.5 min (compare the white and green lines in Fig. 7). The mean change in orientation (measured as the difference in angle of the white and green lines in each subregion) is only 1.6 deg and the standard deviation is 13.9 deg, i.e., there is no large scale change in the fibril orientation. This means that the individual bright Ca II K fibrils are replaced by new ones with very similar orientation and general appearance or, alternatively, the fibrils live longer than the duration of the timeseries while the Ca II K emission disappears and reappears in the same location.

Small-scale evolution is fastest in the strong plage regions while the bipolar region (region D) undergoes the fastest larger scale changes. This is because the small patch of opposite polarity magnetic field changes significantly during the observing sequence. The unipolar regions (e.g., region A) with fibrils extending over several granules and the pore-plage interface (region C) are very stable. The fibril dynamics may be driven by motions in the photosphere. If the granulation and its associated filigree are evolving fast, then the fibrils are more dynamic. This is clearly seen in movies made of the photospheric and chromospheric observations, when watched in parallel.

An example of temporal evolution of photospheric filigree and individual fibrils associated with the filigree is shown in Fig. 14. The region is located close to the edge of the plage. The bright points and filigree are most likely foot points of the Ca II K fibrils seen in the snapshots. The appearance of the photospheric filigree changes during the sequence and at the same time the Ca II K fibrils become gradually brighter and more elongated. A rough estimate of the elongation speed is $\approx$20 km s$^{-1}$. After a couple of minutes the elongated fibrils fade away. Other examples of elongating fibrils with similar speeds are found at the edges of the plage.

Individual fibrils in the plage undergo changes in visibility, but overall the structure changes only little during 3.5 min (Fig. 15). The largest changes are in the underlying granulation pattern which alters the visibility of the fibrils. Some of the fibrils merge and split intermittently. Their orientation can also change slightly. In contrast, the long fibrils extending over the quiet Sun tend to fade away (instead of merging and splitting) and do not show changes in orientation. A movie of the Ca II K images around the plage region (on the left in the FOV) shows an outward moving pattern along the fibrils from the plage towards the quiet Sun (no identification of this pattern with photospheric structures can be made). Another type of lateral movement is occasional bright points that appear to be moving along the fibrils. However, all of these points can be identified as photospheric bright points shining through. It is not possible to say if the fibrils sway in the lateral direction because of the jitter caused by the varying seeing conditions and the slow cadence (15 s) of the data. In general, the average lifetimes of the fibrils are at least 3–4 min which is also the time that the individual fibrils can be tracked reliably. It should be noted that this timescale is similar to the timescale of the underlying granulation.

The general structure of the cusp (region C) remains the same throughout the time series. The patch of opposite magnetic polarity into which the fibrils connect does not disappear during the observing sequence and the individual fibrils, especially the ones connecting to the opposite polarity patch, are long-lived. The time evolution is smooth (they merge, split or fade away) and it is not straightforward to say exactly when a feature is born or dies away. Brightening and darkening of individual points or "crinkles" in the filigree are not well correlated in the photosphere and chromosphere.
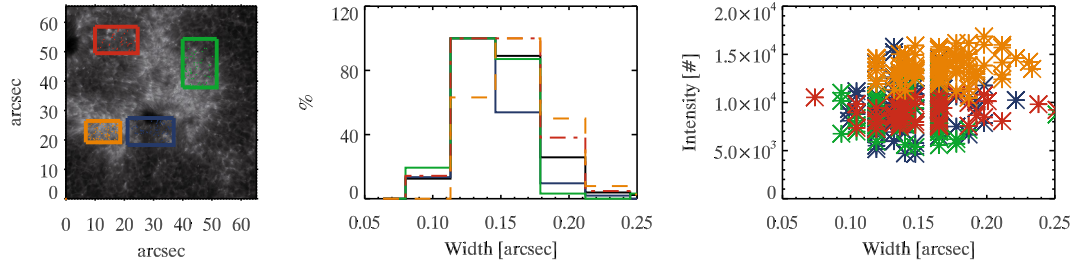
**Fig. 13.** Manually measured fibril widths. First image: colored boxes in the Ca K intensity image show the locations of the four regions where the fibrils with manually measured widths are located. Second image: histograms of fibril widths. Black line is for all four regions, colored lines correspond to the four regions marked in the first image. Third image: scatter plots of fibril widths and intensity. Color coding same as in histograms.
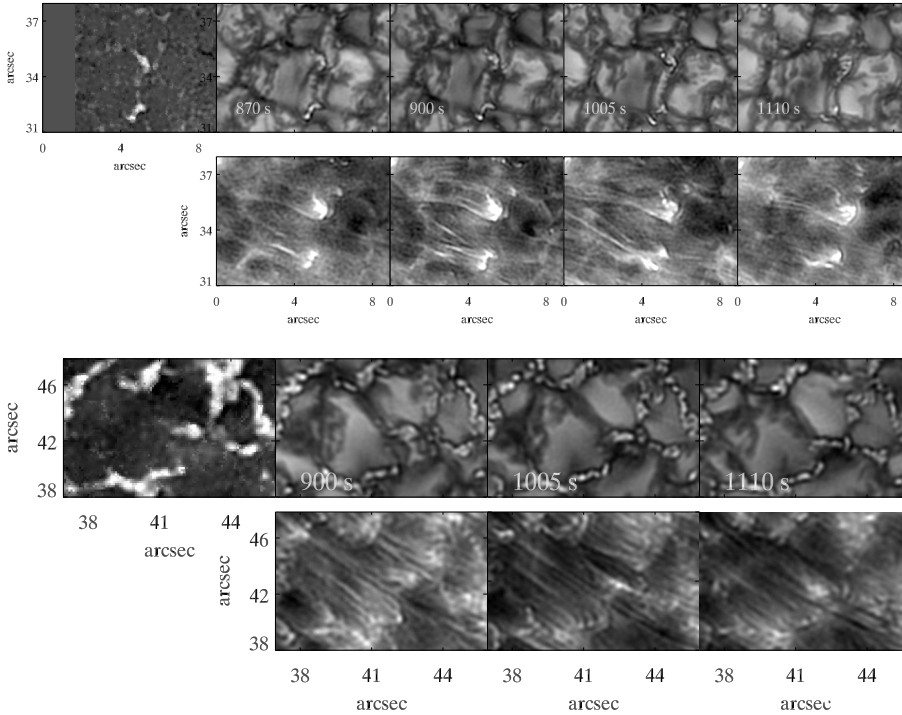


**Fig. 14.** 1st row: longitudinal magnetic flux and continuum snapshots of the same region. Time relative to the beginning of the observing sequence of each snapshot is shown in the corner of each image. 2nd row: Ca II K snapshots corresponding to the continuum snapshots. Note that the images are irregularly spaced in time.
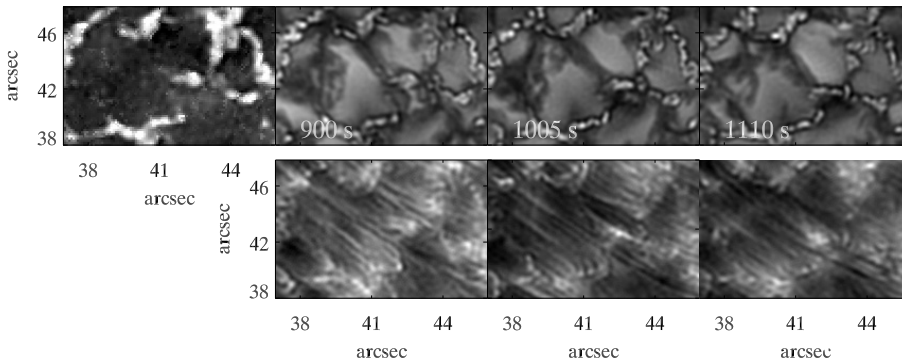


**Fig. 15.** 1st row: longitudinal magnetic flux and continuum snap shots of the same region. Time of each image is shown above each image. 2nd row: Ca II K snapshots taken at the same time as the continuum images.

**Table 1.** Power in regions I, II and III.

| Frequency range mHz | region I: Bright plage | region II: Intermediate plage | region III: Quiet Sun |
|---|---|---|---|
| Continuum | | | |
| 0.4–1.6 | 0.69 | 0.85 | 1.17 |
| 2.4–4 | 0.82 | 0.90 | 1.11 |
| 5.2–8 | 1.02 | 0.97 | 1.01 |
| Ca II K | | | |
| 0.4–1.6 | 0.73 | 1.02 | 1.06 |
| 2.4–4 | 1.12 | 0.85 | 1.06 |
| 5.2–8 | 0.71 | 0.69 | 1.27 |

## 5.1. Power spectra

Power maps of the Ca II K and continuum intensity are plotted in Fig. 16. Shown is a subregion located on the right side of the FOV. The three different frequency ranges (evolutionary, evanescent and propagating) are discussed individually in the following subsections. The evolutionary frequency range encompasses frequencies from 0.4 to 1.6 mHz (periods 10.4 to 41.7 min), evanescent frequency range 2.4–4 mHz (4.2 to 6.9 min) and propagating frequency range 5.2–8 mHz (2.1 to 3.2 min).

### 5.1.1. Evolutionary range <1.6 mHz

In order to compare the power in regions of different chromospheric brightness the FOV of Fig. 16 is divided into three subregions based on the average Ca II K brightness (bright plage: region I in Fig. 16, intermediate plage: region II and quiet Sun: region III). Table 1 shows the amount of power in regions I, II and III relative to the mean power of the entire FOV in each frequency range. In both, the Ca II K and continuum, the brightest plage, which also corresponds to the strongest magnetic flux, has clearly less power in the evolutionary frequency range than the surroundings. There is no difference in Ca II K between regions II and III, but in the continuum there is more power in the quiet Sun (region III) than the weak plage (region II).

The patches of enhanced photospheric power in the left side of the plage (Fig. 16) correspond to the micropores which start to slowly fade away towards the end of the time series. The power enhancement due to the micropores is not visible in the Ca II K image because the plage is dominated by chromospheric emission from the fibrils.

The fibril structure is clearly visible in the low frequencies of the Ca II K intensity power. The individual fibrils are seen as faint bright features which extend beyond the bright plage. This is worth noting, since they are not apparent in the
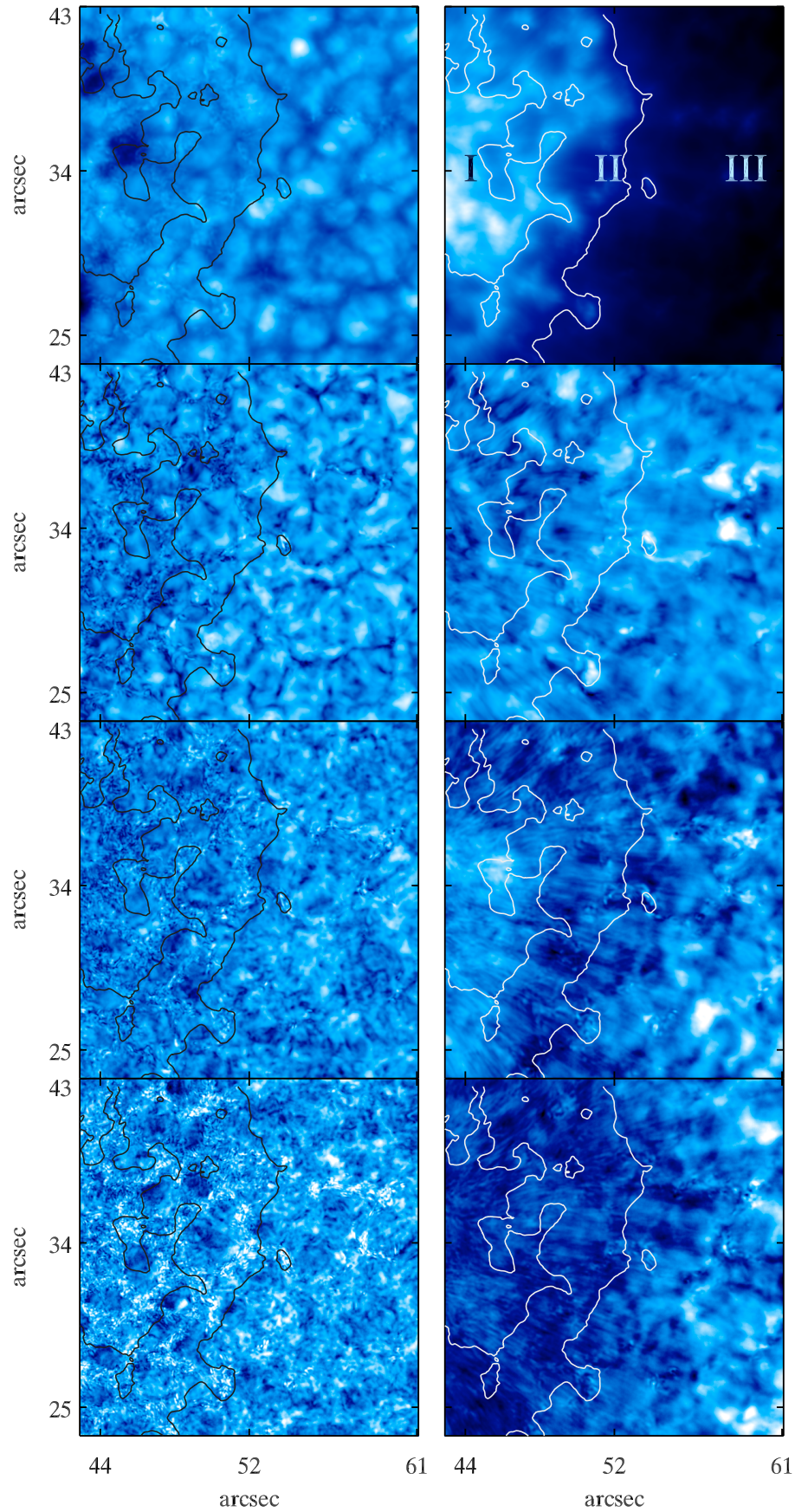
**Fig. 16.** Power maps of a subregion in the FOV. 1st column, 1st row: average of all continuum intensity images with good seeing. The contours outline strong plage (*left* contour region I) and weak plage (*right* contour, region II) relative to quiet Sun (region III) in the Ca II K emission. 2nd row: continuum power at 0.4–1.6 mHz. 3rd row: continuum power 2.4–4 mHz. 4th row: continuum power 5.2–8 mHz. Second column: as first row except for Ca II K. The color scales are chosen to highlight differences in the images.
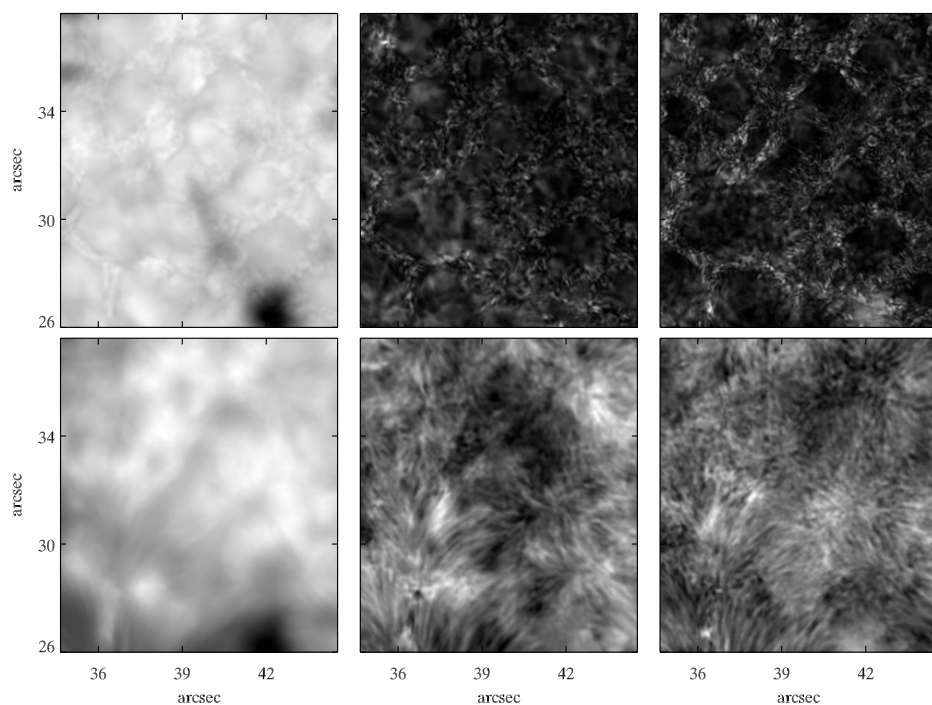
**Fig. 17.** Power map of strong plage. 1st row, 1st image: average continuum intensity. 2nd image: continuum power 2.6–4 mHz. 3rd image: continuum power 5.5–8 mHz. 2nd row as 1st but for Ca II K.

averaged brightness image (top right panel of Fig. 16). The enhanced power may correspond to the gradual brightening and fading away of fibrils. Other regions with increased power are located in the plage at the foot points of the fibrils and in the quiet Sun, where they often correspond to brighter than average intensity and more isolated filigree. The isolated filigree does not appear as bright in the continuum intensity and, consequently, the regions do not exhibit enhanced photospheric power. A local power increase is visible in the superpenumbra of the pore. This corresponds to a sudden brightening seen in Ca II K towards the end of the time series. During the brightening the granulation pattern changes abruptly and a small enhancement is also seen in the continuum power.

### 5.1.2. Evanescent frequencies 2.4–4 mHz

Ca II K power in the evanescent frequencies is suppressed at the edges of the plage (region II) whereas the brightest plage (region I) shows no suppression. In fact, slightly enhanced power in Ca II K is seen by the foot points of the power fibrils. In contrast, region I does not have enhanced power in the photosphere, instead the brightest plage has the least power in this frequency range. This leads to the conclusion that the enhanced power in the bright plage is chromospheric, not photospheric. In the bright plage individual power fibrils are clearly visible in the Ca II K power images (Fig. 17). In fact, they are far better visible in power than in average brightness. Regions of enhanced Ca II K power in the quiet Sun are likely due to the photospheric contribution.

### 5.1.3. Propagating frequencies 5.2–8 mHz

The third frequency range, above the acoustic cutoff frequency, is where the internetwork chromospheric power typically peaks. In the photosphere, the power in this range shows a rapid drop relative to the power of the dominant five-minute periods. Consequently, the photosphere has overall little power in

this range and the spatial pattern in the power map is related to intergranular lanes. In fact, no significant difference is seen between the three regions in the photosphere. Chromospheric power is suppressed both in the bright plage (region I) and the weaker plage (region II). The region of suppressed power extends beyond region II well into region III. Furthermore, individual power fibrils at the plage edge appear as darker structures, i.e., the intensity of the fibrils varies less than the surrounding intensity. Also in strong plage, fibril-like structures are well visible in this frequency range (Fig. 17). Unlike in the evanescent regime, the fibril foot points do not show up as regions of greatly enhanced power. The power enhancement in the propagating range is only modest at the fibril foot points. In contrast, significantly more power is seen in the quiet Sun (region III) in Ca II K.

## 6. Discussion

The current data show that fibrils are a prominent feature in Ca II K. The presence of fibrils indicates that a significant fraction of the signal through this filter is coming from chromospheric structures in these regions. The single most important result of this investigation is that the fibrils in Ca II K are even more abundant and finely structured than ever observed. Prior observations of Ca II K (Beckers 1968; Zirin 1974; Marsh 1976; Rutten 2007) have shown fibrils but not as clearly and in as much detail as in the the current data. The fibrils have not been observed as conspicuously before because of a variety of reasons. Only the Ca II K line core is purely chromospheric, the wings are formed in the photosphere. Since the line core is very dark, relatively few photons originate from the chromosphere. This means that a 1.5 Å filter is probably close to the maximum width at which fibrils outside the strongest plage can be seen. Another factor is the very small apparent fibril width through this broad filter, which leads to very high spatial resolution (and short exposure time) requirements. For ground-based observations these are combined with the need of image reconstruction methods.

Similar structures as the Ca II K fibrils have been observed with the Dutch Open Telescope using a 1 Å wide Ca II H filter (Rutten et al. 2004; Rutten 2007). These bright structures called straws (Rutten 2007) originate from magnetic regions such as active network and plage. They usually coincide with the lower ends of bright Hα fibrils. The straws are qualitatively very similar to the bright Ca II K fibrils, especially in the small patch of network present in the lower right corner of the FOV.

In the observations the bright Ca II K fibrils are seen everywhere in the data where an increased fraction of the signal is coming from the chromosphere. We cannot rule out that if the signal was not dominated by the photospheric contribution in the quiet Sun, the fibrils would be as ubiquitous there as in the vicinity of the plage. In fact, this is rather likely. The fibrils are structured by the underlying magnetic field and the bright endpoints are clearly cospatial with the magnetic concentrations in the photosphere. This is not as obvious in the strong plage where the density of the fibrils is high enough to make identifying the endpoints difficult. In the plage where there is more magnetic flux and due to unipolar crowding the field is more vertical, the fibrils are more vertical and form a carpet covering the surface. Towards the edge of the plage the fibrils become longer and more organized. At the edge they extend radially away from the magnetic concentrations and are nearly parallel to one another. The long fibrils extend over several granules and form a multi-layer (in the sense that not all the fibrils are at the same height) canopy over the outer part of the plage and the quiet Sun.

Since the fibrils appear bright in the Ca II K emission, this indicates a temperature enhancement in the chromospheric layers where the Ca II K line is formed in (e.g., Fig. 1). Why the general structure in the Ca II K emission consists of fibrils instead of a more uniform, homogeneous structure is an interesting question. The fibrils are clearly closely related to the magnetic field and it seems plausible that they outline the general magnetic field structure as proposed by Veeder & Zirin (1970). Perhaps the lower boundary of the field is similar to a corrugated sheet where the Ca II K fibrils are material with sufficient opacity in the dips of the sheet coinciding with the formation range of the line. Another possible explanation is that the magnetic canopy itself is rather homogeneous and some of the magnetic field lines have an enhanced optical depth because they are either more heated or are filled with more material than other field lines. This would result in a visible canopy-structure formed of individual fibrils. Non-uniform heating of the canopy may be due to reconnection or waves. If the differential heating mechanism is waves, the question arises why are the waves excited so locally or why are they channeled only by a portion of the magnetic field lines.

Another question is why do the fibrils remain narrow, coherent structures when the magnetic field, and hence also the fibrils, are expected to expand with height? The combination of noise and threshold may partially explain this: at the foot points the full width of the fibrils is seen, but with increasing distance the fibrils become darker and only the bright core is visible while the fainter edges are drowned in the background noise. Since the contribution function of the filter used in the observations is wide, the background noise (i.e., photospheric contribution) is strong and only the brightest central part of the fibrils is above the noise level. This would also explain why the quiet Sun fibrils are narrower than the fibrils in the plage.

The fibrils extending over the quiet Sun fade gently out of view. This could be because as the magnetic field expands it moves to higher atmospheric layers and, consequently, outside the range of formation of the Ca II K line. Alternatively, the heating mechanism may be more concentrated at the foot points of the fibrils.

Regardless of the speculations above, the Ca II K fibrils support the presence of a hot magnetic canopy (e.g., Solanki et al. 1991; Solanki et al. 1994; Ayres 2002). Furthermore, the coherence of the fibrils lends support to the classical picture of the magnetic canopy (e.g., Jones & Giovanelli 1982; Solanki & Steiner 1990; Bianda et al. 1998) in contrast to the picture where magnetic concentrations in the internetwork disrupt the formation of a coherent large-scale canopy (Schrijver & Title 2003). These two scenarios need not necessarily exclude each other entirely. It may be that the small scale magnetic loops and structures are mostly restricted to the photosphere and/or low chromosphere whereas the canopy is located higher up in the chromosphere. It may also be that the truly quiet Sun lacks a canopy while in other more active regions, such as in the vicinity of chromospheric network, a canopy is present.

The power maps of the Ca II K intensity are very similar to the power maps of Ca II 8542 Å velocity studied by Vecchio et al. (2007). The role of the fibrils in the dynamics is two-fold: firstly, they are associated with the channeling of low (below acoustic cutoff) frequency waves propagating into the chromosphere (e.g., Jefferies et al. 2006). An inclined magnetic field lowers the effective gravity and also the acoustic cutoff frequency of a wave propagating along the field line (Bel & Leroy 1977). Indications of this effect are seen in the power maps (Fig. 16) where the foot points of the fibrils appear as regions of enhanced power in the frequency regime normally evanescent in the chromosphere. The more inclined the field is, the more the acoustic cutoff frequency is lowered. This may explain the long periods in the nearly horizontal fibrils originating from the plage edge. Similar oscillation properties have been observed in e.g. Hα fibrils: long periods (up to ten minutes) are found in the nearly horizontal mottles while the more vertical dynamic fibrils are dominated by periods of four to six minutes (de Pontieu et al. 2007a).

In the present observations the largest enhancement of power at frequencies below the acoustic cutoff is not in the region with strongly inclined field at the edge of the plage, but rather in the strong plage, where the fields are expected to be more vertical. This is not in agreement with the classical picture of better propagation in more inclined fields. Since the photospheric power is not enhanced in the region, the chromospheric enhancement cannot be due to a more efficient excitement of these waves. Consequently, either such oscillations are better visible in more vertical magnetic structures, or there are as yet unknown reasons for their more efficient propagation along nearly vertical fields. The former may be partly explained if at the edge of the plage region the lower parts of the atmosphere contribute significantly to the observed signal, i.e., there is less opacity in the fibrils than the underlying atmosphere and, consequently, we mostly observe the suppression of oscillations from below instead of wave propagation along the fibrils. In addition, if the wavelength of the oscillations is significantly longer than the fibril width, then there is only little change in optical depth due to the wave in nearly horizontal fibrils. In contrast, in the more vertical fibrils the wave changes the properties of the fibril over the full optical depth range of the line formation. If the oscillations are guided by magnetic fields, then the amount of apparent power may also depend on the number of bright points. The greater number of bright points in region I with respect to region II would then imply a larger leakage, and hence also power, in region I.

Furthermore, because of the wide contribution function of the filter, the signal is entirely dominated by the photosphere unless there is additional heating present in the chromosphere.

If such a heating mechanism operates mostly in the vicinity of strong flux concentrations, we would not expect to see the more spatially sparse horizontal fibrils as clearly as the fibrils in the strong plage. One can also speculate whether the waves loose some of their energy through mode conversion when they encounter a large (compared to the wavelength) magnetic field (i.e. the wave-guide) curvature as the field becomes more horizontal at the edge of the plage. This would be similar to what is seen in simulations of coronal loops, where curved structures lead to increased leakage of both sausage and kink waves (Smith et al. 1997; Selwa et al. 2007). Yet another alternative explanation for the lowered acoustic cutoff frequency involves radiative cooling. A loose reasoning can be made where the more inhomogeneous plage region has a shorter radiative cooling time which in turn leads to a decreased acoustic cutoff frequency (Centeno et al. 2006).

The second role the fibrils have in the dynamics is that they act as a canopy over the quiet Sun. The canopy suppresses oscillations from below as is seen in the power map of the propagating frequency regime (last panel in Fig. 16). Recently observational evidence supporting the canopy scenario has increased significantly, e.g., Vecchio et al. (2007) find evidence for it in Ca II 8542 Å data and Holzreuter & Stenflo (2007) in scattering polarization data. Suppression of oscillations in the vicinity of magnetic network was reported by McIntosh & Judge (2001) in SOHO/SUMER data. They referred to the phenomenon as "magnetic shadows". Magnetic shadows in Ca II K have been reported before by Tritschler et al. (2007), Wöger et al. (2006), Reardon et al. (2007). Both the canopy and magnetic shadows are most likely manifestations of the same phenomenon: inclined magnetic fields above quiet Sun regions altering the propagation of waves (McIntosh & Judge 2001; Vecchio et al. 2007). The current high spatial resolution data demonstrate that the canopy is very inhomogeneous and composed of structures with sizes near the currently accessible spatial resolution. This is not obvious in observations with lower spatial resolution.

The effect of the canopy in the very quiet Sun cannot be determined since the signal in these regions is probably coming from much lower (i.e., the chromospheric contribution is very small) and also the canopy (in the current context defined as strongly inclined fibrils that can alter the dynamics of upward propagating waves) is probably located higher up. The Ca II K fibrils are not visible above the quiet Sun: the magnetic field that outlines the fibrils may be above the formation height of the line or the fibrils may not have sufficient density and/or temperature above the quiet Sun. Simultaneous observations with Hα and Ca II K with a narrower filter than the one used here are needed to better understand what happens to the Ca II K fibrils above the quiet Sun.

Unlike Hα dynamic fibrils most of the Ca II K fibrils do not have well-defined endpoints even in the plage. This may be because the fibrils (or perhaps more precisely the portion of the fibrils that is visible in Ca II K) are not in direct contact with the transition region and the abrupt change in temperature associated with it. This scenario has been proposed to explain why most of the nearly horizontal Hα quiet Sun fibrils do not have clearly defined tops (de Pontieu et al. 2007a).

Many of the properties of the Ca II K fibrils are similar to fibrils observed in other spectral lines, such as Hα and Ca II 8542 Å. The similarity of lengths and life times of Hα and Ca II K fibrils was already noted by Marsh (1976). For example, also Hα fibrils (de Pontieu et al. 2007a) and Ca II 8542 Å fibrils (Vecchio et al. 2009) are more dynamic in plage and active network than in the quiet Sun. The dynamics of individual fibrils are also similar: fibrils merge, split, fade away, etc. Since most of the Ca II K fibrils lack a well-defined top it is difficult to measure velocities to see if they follow ballistic trajectories like many fibrils in Hα do (de Pontieu et al. 2007a). The estimate of the Ca II K fibrils elongation speed, 20 km s$^{-1}$, is in the velocity range observed in Hα (de Pontieu et al. 2007a). Large scale movement along the fibrils away from magnetic concentrations is seen in Ca II 8542 Å fibrils data as well (Cauzzi et al. 2008).

The main difference between the Ca II K fibrils and other observations lies in the width of the fibrils. The Ca II K fibrils are very narrow, the average width being near the diffraction limit. One of the more recent quotations on widths of dynamic fibrils seen in Hα is 310 km (0.43 arcsec, de Pontieu et al. 2007b). Spicules seen in Hinode SOT Ca II H data have widths of roughly 200 km, i.e., still larger than the Ca II K widths. The width of the SOT spicules, however, is set by the spatial resolution of the instrument. The discrepancy between Hα and Ca II K may come from the fact that the Ca II K fibrils are a separate structure from Hα fibrils. Alternatively, the horizontal extent of the emitting region might be smaller in Ca II K than in Hα. Finally, the relatively broad filter available for the present observations may limit the apparent widths of the fibrils, since only little contribution is obtained from the chromospheric layers and only the bright spines of the fibrils are seen.

The Ca II K fibril width is related to the general magnetic topology (e.g., brightness and length of fibrils) of the region but not to the intensity of the fibrils. The wider fibrils in regions B (plage) and D (weak plage) may be due to one or a combination of following possibilities: a) noise: the faint fibrils extending over the quiet Sun are more easily overshadowed by the photospheric signal than the bright plage fibrils; b) the larger width in the plage is a superposition effect; c) the plage measurements were made at the base of the fibrils where the fibrils (or at least the emitting regions) are larger if one assumes that the fibrils (not the flux tubes) become narrower with increasing distance from the foot point. This scenario would take place for example if the fibrils get drowned in the background signal as discussed previously. Similar spatial dependence is seen in dynamic Hα fibrils, where the median width in the plage is slightly higher than at the edges of the plage (0.48 and 0.40 arcsec, respectively; de Pontieu et al. 2007b).

The present observations show that the Ca II K chromosphere is not as different from Hα as first might appear but they also raise interesting questions; e.g. it is unclear how exactly the Ca II K fibrils are related to fibrils in other spectral lines. For example, are these the low-height equivalent of Hα? Or are they the same structure? Are the Ca II K fibrils driven by magnetoacoustic shocks like a subset of the Hα dynamic fibrils (Hansteen et al. 2006)? This would explain why a large portion of the Ca II K fibrils tend to recur in the same location whereas the other frequently proposed explanation, i.e., reconnection (e.g., Uchida 1969), does not naturally account for the recurrence. It is not unreasonable to conjecture that Ca II K fibrils may also come in two varieties like the Hinode SOT Ca II H spicules (de Pontieu et al. 2007b), i.e., one consistent with the shock scenario and the other more in line with reconnection. To answer these questions more observations, preferably with a narrower filter or full spectra and simultaneously with other spectral lines, are needed.

## 7. Summary

We have presented high resolution observations of the Ca II K line which show that very narrow fibrils are a prevailing feature

in regions where the chromospheric signal is increased. Based on cotemporal continuum and nearly cotemporal magnetic field observations it is clear that the fibril foot points originate from photospheric magnetic concentrations. The fibrils share many characteristics, e.g. lifetime and dynamics, with fibrils observed in other chromospheric spectral lines. They play an important role in the dynamics: in the plage they channel low frequency waves into the chromosphere while in the more quiet regions the highly inclined fibrils form a layered canopy that suppresses oscillations from below.

# References

Ayres, T. R. 2002, ApJ, 575, 1104
Beckers, J. M. 1968, Sol. Phys., 3, 367
Bel, N., & Leroy, B. 1977, A&A, 55, 239
Bianda, M., Stenflo, J. O., & Solanki, S. K. 1998, A&A, 337, 565
Carlsson, M., & Stein, R. F. 1997, ApJ, 481, 500
Carlsson, M., Hansteen, V. H., de Pontieu, B., et al. 2007, PASJ, 59, 663
Cauzzi, G., Reardon, K. P., Uitenbroek, H., et al. 2008, A&A, 480, 515
Centeno, R., Collados, M., & Trujillo Bueno, J. 2006, ApJ, 640, 1153
Cheung, M. C. M., Schüssler, M., & Moreno-Insertis, F. 2007, A&A, 461, 1163
de Boer, C. R. 1996, A&AS, 120, 195
de Pontieu, B., Hansteen, V. H., Rouppe van der Voort, L., van Noort, M., & Carlsson, M. 2007a, in The Physics of Chromospheric Plasmas, ed. P. Heinzel, I. Dorotovič, & R. J. Rutten, ASP Conf. Ser., 368, 65
de Pontieu, B., McIntosh, S., Hansteen, V. H., et al. 2007b, PASJ, 59, 655
Fontenla, J. M., Avrett, E. H., & Loeser, R. 1993, ApJ, 406, 319
Hansteen, V. H., De Pontieu, B., Rouppe van der Voort, L., van Noort, M., & Carlsson, M. 2006, ApJ, 647, L73
Holzreuter, R., & Stenflo, J. O. 2007, A&A, 467, 695

Janssen, K., & Cauzzi, G. 2006, A&A, 450, 365
Jefferies, S. M., McIntosh, S. W., Armstrong, J. D., et al. 2006, ApJ, 648, L151
Jones, H. P., & Giovanelli, R. G. 1982, Sol. Phys., 79, 247
Lagg, A., Woch, J., Krupp, N., & Solanki, S. K. 2004, A&A, 414, 1109
Marsh, K. A. 1976, Sol. Phys., 50, 37
McIntosh, S. W., & Judge, P. G. 2001, ApJ, 561, 420
Patsourakos, S., Gouttebroze, P., & Vourlidas, A. 2007, ApJ, 664, 1214
Puschmann, K. G., & Sailer, M. 2006, A&A, 454, 1011
Reardon, K. P., Cauzzi, G., & Rimmele, T. 2007, in The Physics of Chromospheric Plasmas, ed. P. Heinzel, I. Dorotovič, & R. J. Rutten, ASP Conf. Ser., 368, 151
Rutten, R. J. 2007, in The Physics of Chromospheric Plasmas, ed. P. Heinzel, I. Dorotovič, & R. J. Rutten, ASP Conf. Ser., 368, 27
Rutten, R. J., Hammerschlag, R. H., Bettonvil, F. C. M., Sütterlin, P., & de Wijn, A. G. 2004, A&A, 413, 1183
Rybicki, G. B., & Hummer, D. G. 1991, A&A, 245, 171
Rybicki, G. B., & Hummer, D. G. 1992, A&A, 262, 209
Scharmer, G. B., Dettori, P. M., Lofdahl, M. G., & Shand, M. 2003b, in Innovative Telescopes and Instrumentation for Solar Astrophysics, ed. S. Keil, & S. Avakyan, Proc. SPIE, 4853, 370
Scharmer, G. B., Bjelksjo, K., Korhonen, T. K., Lindberg, B., & Petterson, B. 2003a, in Innovative Telescopes and Instrumentation for Solar Astrophysics, ed. S. Keil, & S. Avakyan, Proc. SPIE, 4853, 341
Schrijver, C. J., & Title, A. M. 2003, ApJ, 597, L165
Selbing, J. 2005, Master's Thesis, Stockholm Observatory
Selwa, M., Murawski, K., Solanki, S. K., & Wang, T. J. 2007, A&A, 462, 1127
Smith, J. M., Roberts, B., & Oliver, R. 1997, A&A, 317, 752
Solanki, S. K., & Steiner, O. 1990, A&A, 234, 519
Solanki, S. K., Steiner, O., & Uitenbroeck, H. 1991, A&A, 250, 220
Solanki, S. K., Livingston, W., & Ayres, T. 1994, Science, 263, 64
Title, A. M., & Rosenberg, W. J. 1981, Optical Engineering, 20, 815
Tritschler, A., Schmidt, W., Uitenbroek, H., & Wedemeyer-Böhm, S. 2007, A&A, 462, 303
Uchida, Y. 1969, PASJ, 21, 128
Uitenbroek, H. 1998, ApJ, 498, 427
van Noort, M., Rouppe van der Voort, L., & Löfdahl, M. G. 2005, Sol. Phys., 228, 191
Vecchio, A., Cauzzi, G., Reardon, K. P., Janssen, K., & Rimmele, T. 2007, A&A, 461, L1
Vecchio, A., Cauzzi, G., & Reardon, K. P. 2009, A&A, 494, 269
Veeder, G. J., & Zirin, H. 1970, Sol. Phys., 12, 391
Weigelt, G. P. 1977, Opt. Comm., 21, 55
Withbroe, G. L. 1983, ApJ, 267, 825
Wöger, F., Wedemeyer-Böhm, S., Schmidt, W., & von der Lühe, O. 2006, A&A, 459, L9
Zirin, H. 1974, Sol. Phys., 38, 91